DTU Library

Water-based devices for advanced control of electromagnetic waves

Jacobsen, Rasmus E.; Arslanagic, Samel; Lavrinenko, Andrei V.

Link back to DTU Orbit

Water-based devices for advanced control of electromagnetic waves

Rasmus E. Jacobsen, Samel Arslanagić and Andrei V. Lavrinenko

COLLECTIONS

F   This paper was selected as Featured

View Online   Export Citation   CrossMark

ARTICLES YOU MAY BE INTERESTED IN

Molecular dopants: Tools to control the electronic structure of metal halide perovskite interfaces
Applied Physics Reviews **8**, 041301 (2021); https://doi.org/10.1063/5.0060129

Anisotropic non-split zero-energy vortex bound states in a conventional superconductor
Applied Physics Reviews **8**, 031417 (2021); https://doi.org/10.1063/5.0055839

Metal-based nanoparticles for combating antibiotic resistance
Applied Physics Reviews **8**, 041303 (2021); https://doi.org/10.1063/5.0060299

Water-based devices for advanced control of electromagnetic waves 🅕

Rasmus E. Jacobsen,[1,2,a)] 🆔 Samel Arslanagić,[2,b)] 🆔 and Andrei V. Lavrinenko[1,c)] 🆔

AFFILIATIONS

[1]Department of Photonics Engineering, Technical University of Denmark, Bld. 345A, Ørsteds Plads, 2800 Kgs. Lyngby, Denmark
[2]Department of Electrical Engineering, Technical University of Denmark, Bld. 348, Ørsteds Plads, 2800 Kgs. Lyngby, Denmark

[a)]rajac@elektro.dtu.dk
[b)]sar@elektro.dtu.dk
[c)]Author to whom correspondence should be addressed: alav@fotonik.dtu.dk

ABSTRACT

Tunable devices are of great interest as they offer reconfigurability to their operation, although many of them employ rare and expensive materials. In a world with increasing focus on ecological compatibility and recyclability, immense efforts are being made to find bio-friendly alternatives. However, in some cases, one does not have to look far, because water, a high-permittivity dielectric at microwave frequencies, is readily available. Recent studies have shown that compact Mie resonators, which are the fundamental blocks in all-dielectric metamaterials and dielectric resonator antennas, can be realized with small water elements. In a variety of applied physics areas, encompassing frequencies from the radio to the optical parts of the spectrum, all-dielectric implementations have received immense attention. When it comes to water, its temperature-dependent permittivity and liquidity enable a multitude of unprecedentedly simple means to reconfigure and tune the resulting devices. Moreover, being a polar solvent, water easily dissolves various physiologically important electrolytes, which potentially can be exploited in a sensor design. Presently, we review water-based devices for advanced microwave control and sensing. We show and discuss the dynamic properties of water and examine the microwave scattering and absorption characteristics of single water elements. We investigate how such water elements can be employed in various microwave designs, including single resonators, metamaterials, metasurfaces, antennas, absorbers, and radio frequency components. The main complications of water are its losses, especially at higher microwave frequencies, and its stability. We discuss how to overcome these and show that even highly loss-sensitive modes, namely, toroidal modes and bound states in the continuum, can be realized with water-based devices. We believe that water-based devices usher the route to meet the UN proclaimed goals on global sustainability and human-friendly environment.

TABLE OF CONTENTS

I. INTRODUCTION

Water—covering more than two thirds of Earth's surface, vital for all life, known as "the universal solvent," etc.—is perhaps the most important and unique substance in our world.[1–3] Although the most studied inorganic compound, scientists continue to dwell upon the remarkable properties of water[4–15] and yet some remain mysteries.[16] Water's unique properties stem from the arrangement of its polar molecules. The water molecule constitutes an asymmetric alignment of one negatively charged oxygen atom (O^-) and two positively charged hydrogen atoms (H^+). A sketch of the water molecule is shown in Fig. 1(a). The atomic positioning forms two even but oppositely charged poles, i.e., a permanent dipole. In the liquid state, the water molecules (or dipoles) react to an applied electric field through their alignment with the field, thereby polarizing the bulk water. As the water molecules are very densely spaced, the polarization mechanism
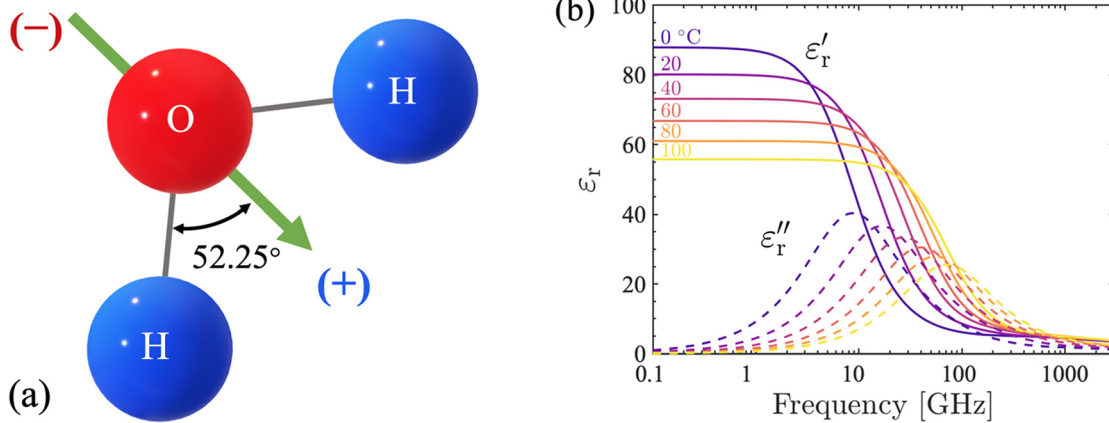
FIG. 1. (a) Sketch of a water molecule with the poles and dipole moment (green arrow). (b) Relative permittivity of water as a function of frequency for temperatures from 0 °C to 100 °C. The permittivity model includes three relaxation processes and is taken from Ref. 9.

provides water an exceptionally high polarization vector even in small and compact volumes, such as protein pockets.[8] With no applied electric field, the orientations of the permanent molecular dipoles are random, resulting in zero net polarization. The polarization properties of water are typically described by its complex relative permittivity (dielectric function) $\varepsilon_r = \varepsilon_r' + i\varepsilon_r''$, which is shown in Fig. 1(b), and depend on dynamic parameters, such as frequency of the electric field and water temperature.[9] Unlike that of many other polar substances, the permittivity of water is notable even at GHz frequencies. In 2015, inspired by Rybin *et al.*[17] as well as Popa and Cummer,[18] Andryieuski *et al.* demonstrated for the first time the possibilities with exploiting water's dynamic properties in microwave all-dielectric metasurfaces (MSs).[19] This launched a series of publications on water-based (WB) microwave devices, such as tunable metamaterials (MMs)[20–23] and MSs,[24–33] as well as MS reflectors,[34–38] MS absorbers,[39–71] and many more;[72–79] see Table I for a thorough overview. While the recent efforts on WB MSs have certainly given new life to water as an interesting microwave material, it must be mentioned that its use within the area of microwave antennas, with the first antenna dating back to 1999,[80] has been around for many years and still constitutes an active research field;[80–126] see Table I for more details on particular antenna types. A very detailed review of water- and other liquid-based antennas is given in Ref. 127. In addition, switching of guided waves on a coplanar waveguide with a water drop was demonstrated in 2007.[128] Recently, new applications of water have been presented including a radio frequency (RF) tuner[129] and a bound state in the continuum (BIC) structure.[130] The latter concerns an important concept, known from quantum physics and extended to acoustics and photonics, which has recently been realized in a simple microwave single-resonator structure well-suited for advanced microwave sensing of water. In general, WB devices exploit the high permittivity of water to tailor the phase and amplitude of microwave fields by invoking strong field intensities in the bulk water volumes. In fact, such high-permittivity bodies are known to exhibit Mie resonances (see, e.g., Refs. 131 and 132) which are the driving mechanisms behind dielectric resonators used in dielectric resonator antennas[133] as well as all-dielectric MMs and MSs.[134]

A major difference between water and conventional microwave dielectrics is its liquid state at room temperature which, in general,

holds a major advantage: water simply takes up the shape of the container it is put in. With the recent progress of 3D printers, it is possible to produce routinely complex and flexible structures with cavities (see, e.g., Refs. 40 and 52) otherwise extremely challenging with, e.g., high-permittivity ceramics. A simple redistribution, reshaping, and/or

TABLE I. Overview of water-based devices.

Device	Type	References
Single resonators	General study	72–76, 78, 79
	MRI	77, 135
	BIC sensor	130
Metamaterial	Non-resonant	23
	Negative index	21
	Topological transitition	22
	Fano resonance	17
	Material phase study	20
Metasurface	Absorber	39–71
	Reflector	34–38
	Toroidal mode	32
	Sensor	136
	All-dielectric	24–31
	Water/metal	33
Antenna	Monopole	81–86, 92, 103, 114, 123–126
	DRA	80, 87–91, 93–101, 119, 120
	Helical	102, 104
	Patch	105–108
	Microstrip loading	109–113, 115
	Hybrid	116
	Array	117, 122
	Yagi-Uda	118, 121
RF components	Switch	128
	Tuner	129

temperature shift of water alters the system response in the form of a perturbation of the local fields, frequency shift, and/or transmission/reflection change. It is also possible to alter the permittivity of water by dissolution of, e.g., electrolytes and salts in it, which offers another route of tuning (see, e.g., Refs. 25, 34, and 92). Furthermore, as water is transparent at optical frequencies, it is possible to make the WB MS visually transparent while blocking or absorbing microwaves (see, e.g., Refs. 44, 60, and 70). The abundance, low cost, bio-friendly nature, and dynamic properties of water make it a very interesting alternative component for extremely cheap, simple, green versatile microwave systems, albeit the losses at higher frequencies limit the total efficiency in non-absorbing devices. WB microwave devices cover a wide range of applications, such as electromagnetic waves absorption, beam-steering, radar cross section (RCS) reduction, antennas, radomes, circuit components, heating, and sensing.

The purpose of the present work is to provide an overview of the properties of WB microwave devices and the pros and cons of their applications. The manuscript is organized as follows. Section II introduces and discusses the permittivity model of water as well as the power absorption in lossy dielectrics, as this plays a major role in the performance of the WB devices. In Sec. III, we investigate the resonant properties of a single spherical water element and an array of such elements to shed light on the fundamental characteristics of simple WB MSs. Subsequently, we present and discuss a variety of WB MMs and MSs with a range of functionalities, such as wideband absorption as well as tunable reflection and transmission control. In Sec. IV, various WB antennas are discussed including a transparent patch antenna and a Huygens antenna for increased focusing of the radiated power. WB RF components including a coplanar waveguide switch and an RF tuner are presented in Sec. V. In Sec.VI, we show WB structures utilizing peculiar modes, such as toroidal modes and BICs. The latter represents our very recent work showcasing how water can be exploited for symmetry-breaking of a BIC. At last, we discuss the applications and outlook of WB devices in Sec. VII.

II. PERMITTIVITY OF WATER

The permittivity of water fits the single relaxation Debye model with a good approximation from static to 50 GHz at room temperature (see, e.g., Ref. 15 for an overview of permittivity models). However, recent studies show that the underlying reorientation of water molecules is not Brownian motions, but discontinuous "jumps," when an appropriate defect occurs in the hydrogen network.[6,7,15] Furthermore, the Debye model ignores the dipole–dipole interaction, which is also considered to be incorrect. Still, the experimental data can be fitted very well with the Debye model. Ellison[9] presented a very useful analytical model of the permittivity based on the fitting of experimental data for frequencies from static to 25 THz and temperatures 0–100 °C. Presently, we provide Ellison's simplified permittivity model based on three relaxation processes fitted for frequencies from DC to 3 THz for temperatures 0–100 °C,

$$\varepsilon_r(\omega, T_w) = \varepsilon_s(T_w) + i\omega \sum_{n=1}^{3} \frac{\varepsilon_{\infty,n}(T_w)\tau_n(T_w)}{1 - i\omega\tau_n(T_w)}, \quad (1)$$

assuming the time factor $\exp(-i\omega t)$ with t being the time, ω – the angular frequency, and T_w – the temperature given in °C. The static permittivity $\varepsilon_s(T_w) = 87.9 - 0.404T_w + 9.59 \times 10^{-4}T_w^2 - 1.33 \times 10^{-6}T_w^3$, the optical permittivity $\varepsilon_{\infty,n}(T_w) = a_n\exp(-b_nT_w)$, and the relaxation

time $\tau_n(T_w) = d_n\exp\left(-\frac{T_n}{[T_w+T_c]}\right)$ with the critical temperature $T_c = 132\,°C$. Other constants are provided in Table II.

In Fig. 1(b), we show the frequency and temperature dependence of the relative permittivity of water from 0.1 to 3000 GHz. At low frequencies (<1 GHz), ε_r' is high, while ε_r'' (responsible for material losses) is low. At room temperature (20 °C), the real part is approximately 80 from low frequencies up to 3 GHz. It decreases dramatically at higher frequencies, while the absorption increases and peaks around 20 GHz. The two other relaxation processes start at frequencies above 100 GHz and decrease the permittivity even further.

We see that increasing the temperature of water blue shifts the permittivity spectrum, and at low frequencies, the permittivity decreases. Bringing the water temperature from 0 °C to 100 °C decreases the permittivity from $86.8 + i9.2$ to $55.8 + i0.71$ at 1 GHz. Interestingly, it is often the change in ε_r' that is highlighted, whereas in fact, it is the imaginary part ε_r'', which is more affected by the temperature shift. Despite this, we must emphasize that it is the high ε_r', which allows for the strongly induced fields in the WB devices, thus providing their particular properties.

Adding salts, like, e.g., NaCl, to water, increases the conductivity, effectively corresponding to an increase in ε_r''.[137] This is utilized in some WB devices as a water volume with high salinity responds to electromagnetic fields in a similar way as metals. At frequencies below 20 GHz (and temperature of 20 °C), ε_r'' increases significantly with higher salinity levels, while at higher frequencies ε_r'' is slightly decreased. For all frequencies, ε_r' is reduced with increasing salinity levels.

Next, we present an important aspect of the power absorption in resonant water structures. From Poynting's theorem, one finds that the absorbed electromagnetic power in lossy dielectrics can be determined as[138]

$$P_{\text{abs}} = \frac{\omega\varepsilon_0}{2} \int_{V_w} \varepsilon_r''(T_w)|\mathbf{E}|^2 dV, \quad (2)$$

where ε_0 is the free-space permittivity, $\mathbf{E}$ is the electric field, dV is the infinitesimal volume element, and V_w is the volume of water. Since water can attain different temperatures in its volume, $\varepsilon_r''(T_w)$ is placed inside the integral. We emphasize that P_{abs} is not only proportional to $\varepsilon_r''(T_w)$, but also to $|\mathbf{E}|^2$. At resonance, $|\mathbf{E}|$ is maximum, however, if $\varepsilon_r''(T_w)$ increases, the intensity of the resonance, and therefore, $|\mathbf{E}|$ decreases. For low-loss dielectrics, increasing $\varepsilon_r''(T_w)$ causes a growth in P_{abs} as the intensity is only slightly decreased. For lossy dielectrics, e.g., water, the opposite can happen because the intensity of the electric field is greatly reduced by the losses.

III. METASURFACES AND METAMATERIALS

In this section, we present several WB MSs and MMs, which pave the route toward cheap tunable bio-friendly alternatives for many

TABLE II. Values for the constants in Eq. (1).

n	a_n	$b_n \times 10^{-3}$ (°C^{-1})	d_n (fs)	T_n (°C)
1	79.3	4.33	135	653
2	3.61	10.7	0.365	1220
3	1.97	2.52	5.10	396

microwave applications. In general, they are based on dielectric resonators, also known as Mie resonators, and take the form of small water inclusions in low-dielectric hosts. Therefore, we will start by presenting the case of a single water inclusion, namely, a sphere, and investigate its scattering and absorption characteristics.

A. Mie resonances in single water inclusions

High relative permittivity of water enables realization of compact Mie resonators with high energy extinction. In fact, this is the mechanism behind the Internet parlor trick pertaining the sparking of two cut grape hemispheres inserted into a microwave oven.[78] As an example, let us take the classical case study of a plane wave incidence on a dielectric sphere, which was also investigated in Ref. 74. The water sphere has radius $r_s = 21.6$ mm and temperature $T_w = 20\,^\circ$C and is placed in free space. Of course, the water cannot sustain the spherical shape without being placed in a container; however, there are many solid dielectrics available to this end with permittivities close to that of air in the microwave frequencies, see, e.g., Ref. 139. The spectrum of the scattering and absorption efficiencies is shown in Fig. 2(a). We can divide the spectrum into three parts: I. Below 0.5 GHz, the incident wave passes the sphere nearly unperturbed. II. From 0.5 to 3 GHz, resonances drive the response. III. Above 3 GHz, the water sphere scatters as a metallic object of similar size. We are, of course, interested in the part where the resonances govern. There are several resonances, and their frequencies are controlled by judiciously changing the water amount, shape, and permittivity of the water volume. For example, by increasing the temperature, we effectively reduce the permittivity and thus blue shift the spectrum (see, e.g., Refs. 9, 17, and 90).

According to the Mie theory, different types of multipole modes can be excited in the dielectric sphere. However, due to the losses in water, only dipole modes are excited efficiently, namely, magnetic (**m**) and electric dipoles (**p**) with the first being the most pronounced, see Fig. 2(a). All other modes like quadrupoles or octupoles are suppressed by the losses. Furthermore, the losses cause the high absorption and broadening of the resonances. Two ways to reduce losses (i.e., making ε_r'' smaller) are by either increasing the size of the sphere, corresponding to red shifting the spectrum or increasing the

temperature (see, e.g., Ref. 74) Other types of WB inclusions have been investigated including cylinders,[73] a water-metal hybrid structure,[79] and even more complex shapes.[47,59] Their fundamental electromagnetic properties display various performance characteristics providing a variety of options for the designing of WB devices composed of resonators.

B. Resonances in simple metasurfaces for wave control

All-dielectric MSs are composed of a matrix of high permittivity inclusions in a low permittivity host. First, we show results for a simple all-dielectric WB MS of identical water spheres in Fig. 2(b), similar to a MS proposed in Ref. 19. The lattice constant is $a = 75$ mm, and the radius and temperature are the same as in our example in Sec. III A with a single sphere. We find that the dipole resonances drive the response of the MS and cause a significant change in transmission, reflection, and absorption. Most of the extinct energy is absorbed, but it is not as pronounced as in the case of a single sphere. This is due to the coupling of the spheres, which provides yet another tuning parameter.

By changing the shape of water, it is possible to control the spectrum as demonstrated in Fig. 3(a), where the sphere is stretched/compressed in different ways.[19] Depending on stretching/compression of the water volume, the dipole resonances can be moved spectrally closer to or away from each other. Gravity can also be utilized to control the water shape. By mechanical rotation of the structure with partially filled containers, it is possible to alter the transmission and reflection as shown in Fig. 3(b).[24] The measurements were performed in anechoic conditions, and the MS response to both linear and circular polarizations was investigated. In Fig. 3(c), a MS consisting of rod-like water inclusions in a Rohacell 51 HF host was demonstrated to have switching capabilities through 90° mechanical rotation of the MS.[28] Magnetic dipole resonances were excited in the water inclusions for the original position of the MS (0° rotation angle) resulting in high reflection of the incident wave—the non-transmissive state. Rotating the MS by 90° greatly increased the transmission as no resonances were excited. The experiment was conducted using a rectangular
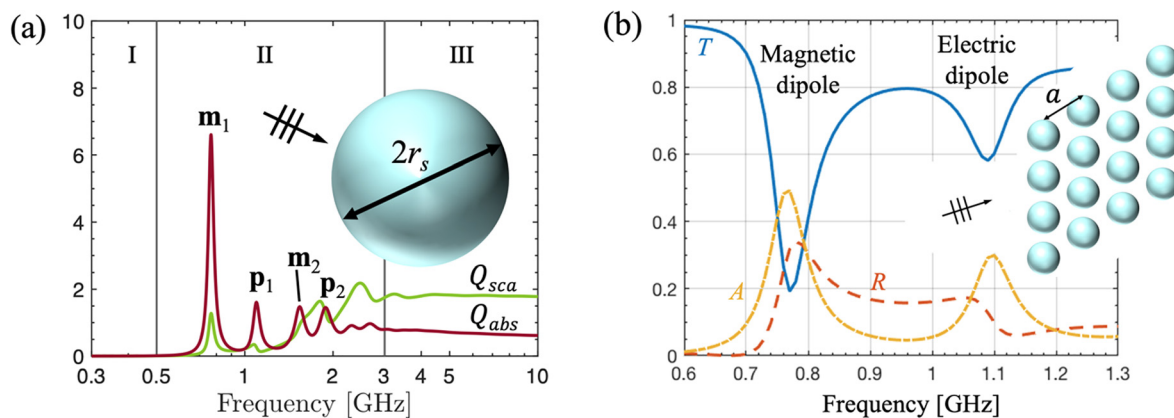
FIG. 2. (a) Scattering and absorption efficiency spectra when a plane wave is incident on a single water sphere (the configuration is shown in the inset). (b) Transmittance (T), reflectance (R), and absorption (A) spectra of a MS consisting of a square lattice of water spheres under normal plane wave incidence. The sphere radius is $r_s = 21.6$ mm, and the lattice constant $a = 75$ mm.
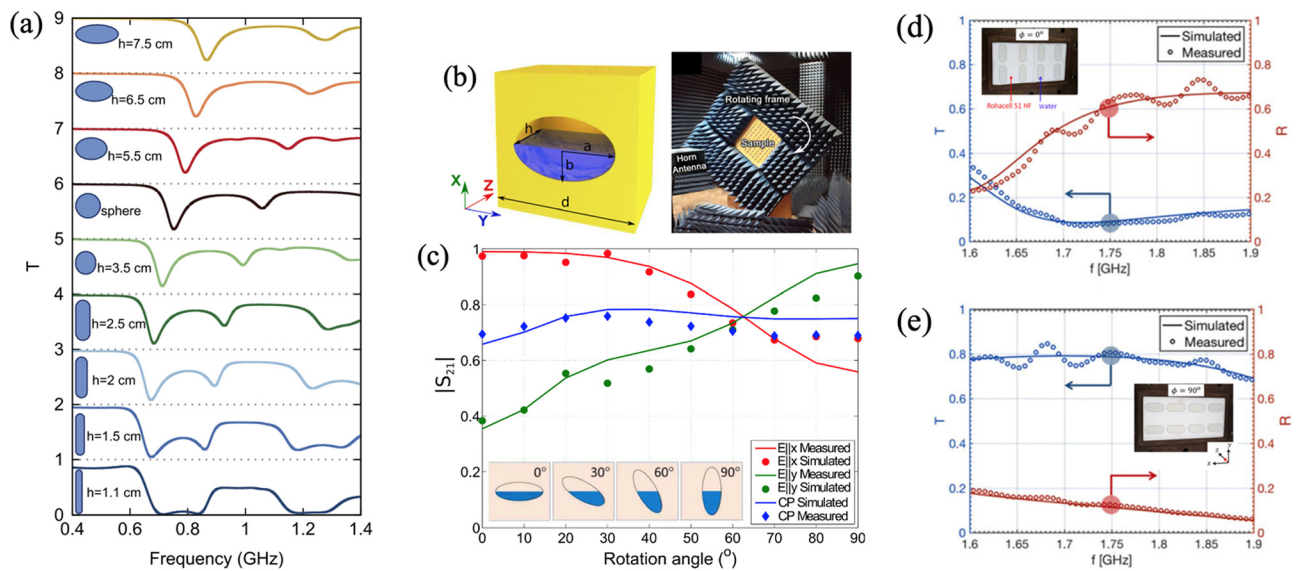
FIG. 3. Control of transmission and reflection with simple WB MSs. (a) Simulated transmittance spectra for a WB MS with different stretching/compressing of its water spheres. The excitation is a linearly polarized plane wave at normal incidence. Reprinted with permission from Andryieuski et al., Sci. Rep. **5**, 13535 (2015). Copyright 2015 Authors, licensed under a Creative Commons Attribution (CC BY) license.[19] (b) and (c) MS with partially water-filled inclusions in foam host. (b) Sketch of one MS element (left) and photograph of the MS putted in the experimental setup (right). (c) The measured and simulated transmission of waves with different polarizations is changed through simple mechanical rotations. Reprinted with permission from Odit et al., Appl. Phys. Lett. **109**, 11901 (2016). Copyright 2016 AIP Publishing.[24] (d) and (e) Measured and simulated reflection and transmission spectra of a MS with rod-like water elements in a Rohacell 51 HF host material. The measurements are performed in a rectangular waveguide, which emulates an infinite periodic extension of the MS. (d) shows the 0° rotation of the MS and (e) the 90° rotation. Insets show the MS placed in a waveguide section. Reprinted with permission from Jacobsen et al., IEEE Antennas Wireless Propag. Lett. **17**, 571 (2018). Copyright 2018 IEEE.[28]

waveguide, which emulated a periodic extension of the MS consisting of only six elements. Furthermore, stacking multiple MSs further decreased the transmission for 0° rotation and increased the transmission for 90° rotation. The latter was provided by the balancing of electric and magnetic dipoles satisfying Kerker's condition, see, e.g., Refs. 132, 140, and 141 for more information about Kerker's condition and small directive scatterers.

The temperature tuning capability of the MSs in Figs. 3(a) and 3(c) was investigated numerically, both depicting a linear frequency blue-shift of around 0.14%/°C and 0.25%/°C, respectively, when increasing from 0 °C to 100 °C.[19,29] Heating of the MS can be done by various stimuli, for example, by light, microwaves, chemical reactions, mechanical friction, and electrical current. All methods make the system more complex, and due to water's exceptional heat capacity, significant energy is required for heating. This is perhaps why experimental studies of temperature tuning of WB MSs are scarce.[17,20,51,65]

C. Metasurface absorbers

Perhaps the most successful application of WB MSs is with absorption of microwaves.[39–71] The high permittivity and losses of water make it an excellent material for both narrow and broadband absorbers, see Fig. 4. The first WB MS absorber was proposed by Yoo et al. in 2015,[39] Figs. 4(a)–4(c). It consisted of distilled water droplets on a FR4 substrate with hydrophobic/hydrophilic surface patterning on the frontside and a ground conducting plane on the backside. The height of the droplets was controlled with simple addition/removal of water effectively changing the absorption bandwidth. Additionally, the

diameter was also adjusted with different hydrophobic/hydrophilic surface patterning. The MS had an absorption bandwidth (absorptivity higher than 90%) that covered 43% of the central frequency, which was achieved with three resonances excited in the MS distributed across its spectrum.

Besides the large absorption bandwidth, WB MS absorbers can function for both TE and TM polarizations as well as for a wide range of incidence angles. Furthermore, they are also less sensitive to temperature-changes compared to other WB devices. As noted previously, water also introduces additional advantages besides those provided by its high permittivity. Some of the WB MS absorbers feature visual transparency,[43,44,60,70] which opens for the possibility of windows for stealth vehicles, vessels, and aircrafts as well as anechoic chambers. WB MSs can also be made flexible as is the case for the MS proposed in Ref. 40, see Fig. 4(d). The flexibility was provided by a dielectric substrate of polymethyl methacrylate (PMMA) host making it possible to cover objects of different shapes with the MS. Similar to Ref. 39, the height of the water drops could be adjusted, albeit here microfluidic channels were used instead, see Fig. 4(e).

More complicated designs have been proposed for further performance enhancement. Recently, a MS composed of 3D printed Swastika-shaped water inclusions has been investigated in Ref. 59 showing an ultrabroadband absorption bandwidth of 136% (9.3–49 GHz), see Fig. 4(f). The MS is made of a polylactic acid host structure with water inclusions connected by fluidic channels. The thickness of the MS is between 1/10 and 6/10 of the free-space wavelength in the frequency operation band. Here, we emphasize that, besides Mie resonances in the water inclusions, other mechanisms
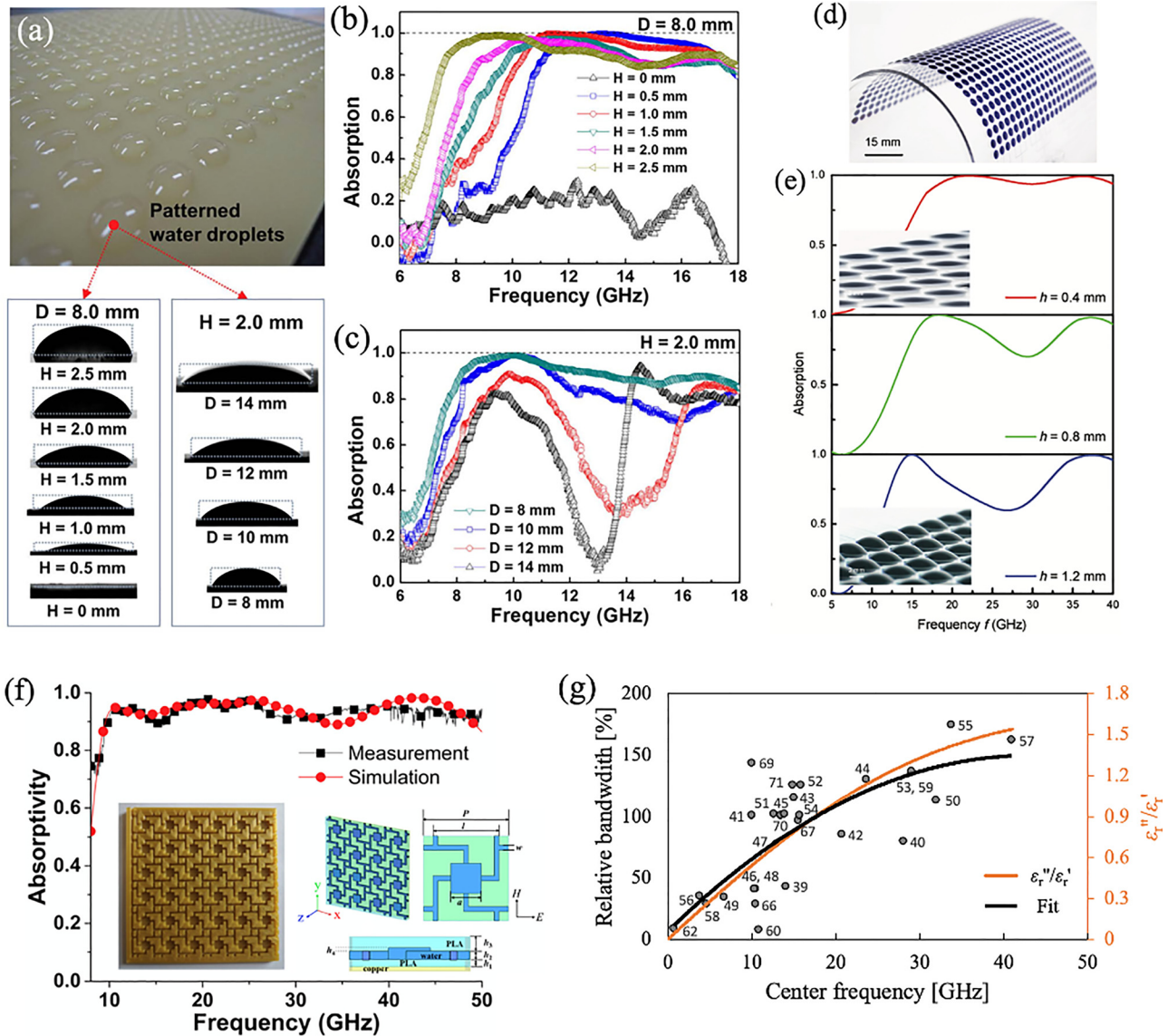
FIG. 4. WB MS absorbers. (a) Photograph of a MS absorber of periodic water droplets. (b) and (c) show the measured absorption spectra for different droplet sizes. Reprinted with permission from Yoo *et al.*, Sci. Rep. **5**, 14018 (2015). Copyright 2015 Authors, licensed under a Creative Commons Attribution (CC BY) license.[39] (d) Photograph and (e) measured absorption spectra of a flexible MS absorber for various water fillings. Adapted with permission from Song *et al.*, Adv. Opt. Mater. **5**, 1601103 (2017). Copyright 2017 John Wiley and Sons.[40] (f) Measured and simulated absorption spectra of a 3D printed Swastika-shaped MS absorber. The insets show a photograph and sketches of the MS. Adapted with permission from Zhang *et al.*, IEEE Antennas Wireless Propag. Lett. **19**, 821 (2020). Copyright 2020 IEEE.[59] (g) 90% absorption relative bandwidth (left *y*-axis) vs the center frequency for different WB MS absorbers in the case of a linearly polarized plane wave at normal incidence and water temperature at 20 °C.[39–60,62,66,67,69–71] The numbers of each point display the references. The loss tangent of water, $\varepsilon_r''/\varepsilon_r'$ (right *y*-axis), as a function of frequency is included in (g).

like, e.g., Fabry–Pérot resonances contribute to the absorption. Simulation results show minimal dependence on changes in water permittivity due to temperature shifts, and thus, the MS can be employed under various conditions as long as the water does not freeze or boils. Furthermore, the absorption efficiency is above 80% for TE (TM) waves with incidence angles below 45° (60°).

A map of the center frequencies and relative bandwidths of all WB MS absorbers operating in the frequency band 0.7–74 GHz is shown in Fig. 4(g). The trend shows that the relative bandwidth increases with the increasing center frequency and follows that of the loss tangent of water ($\varepsilon_r''/\varepsilon_r'$), which has been included in Fig. 4(g), right *y*-axis. As the loss tangent of the water increases, the quality factor of the resonances simply decreases effectively permitting larger relative bandwidths at higher frequencies. We also observe that the curves in Fig. 4(g) predict a maximum of the relative bandwidth at a center frequency around 50 GHz.

A WB MS absorber operating in the THz-regime was recently proposed.[61] The band of potential 90% absorption extended with 66.5% bandwidth is centered around the center frequency of 6.77 THz. The MS consists of water inclusions in a polytetrafluoroethylene (PTFE) layer sandwiched by a biased graphene layer on the top and a gold layer on the bottom. The MS can potentially be tuned dynamically by changing the bias of the graphene layer.

Implementations of WB MS absorbers in microwave systems have been few so far. One has been absorbers in radomes, which are designed to reflect/absorb the frequencies outside the passband.[64,65] Frequency tuning of the WB absorber for radomes by mechanical perturbation and temperature shift of the water volume was demonstrated in Ref. 65.

D. Reflection control with metasurfaces — toward WB reflectarrays

MSs exhibiting anomalous reflection are called MS reflectarrays. They carefully manipulate the amplitudes and phases of the local scattered fields across the MS to tailor the reflected waves at will. This is governed by generalized Snell's law for a structure with the spatial phase variation $\Phi(x,y)$ across its surface[142]

$$\sin\theta_r - \sin\theta_i = \frac{\lambda_0}{2\pi}\frac{\partial^2\Phi(x,y)}{\partial x\partial y}, \tag{3}$$

with θ_i and θ_r being the incidence and reflection angles, respectively, and λ_0 being the free-space wavelength. In MS reflectarrays, subwavelength scatterers, placed across the MS, are used to provide discontinuous phase shifts, effectively changing the reflection angle of the reflected wave. The main task is to find these scatterers providing the required phase shift, while maintaining a high reflection. For example, if an anomalous plane wave reflection is desired, then a periodic linear phase shift of 2π each x and/or $y = \lambda_0$ is required. Many metallic and a few dielectric microwave MS reflectarrays have been demonstrated with very high efficiencies; however, they lag tuning capabilities.[143] Introducing tuning parameters to the systems has shown inevitable efficiency reductions.

Different configurations of WB MS reflectarrays have been used,[34–37] as shown in Fig. 5. The simplest one perhaps is composed of cylindrical water inclusions in a Rohacell 51 HF host backed with a metallic ground conducting plane,[36] see Figs. 5(a) and 5(b). Almost a full 2π phase control was obtained with a magnetic dipole resonance induced in the water cylinders (water temperature of $20\,^\circ$C) through variation of the cylinder height. A supercell of eight elements anomalously reflected a normally incident plane wave at a reflection angle of 51.3°. Nearly all reflected power was channeled into the desired direction, albeit the water losses limited the total reflected power to around 37% of the incident power. Potentially, the MS can be reconfigured for different reflection angles or frequency operation by simply changing the height of water in the cylindrical inclusion or by changing its permittivity (with temperature and/or salinity changes). Since the containers for the water are identical, the number of inclusions in the supercells can be adjusted as well.

Another type of WB MS reflectarray was investigated in Ref. 34, see Figs. 5(c) and 5(d). The MS consisted of a sheet of Teflon woven glass (F4B) with a metal coding pattern backed with a saline water
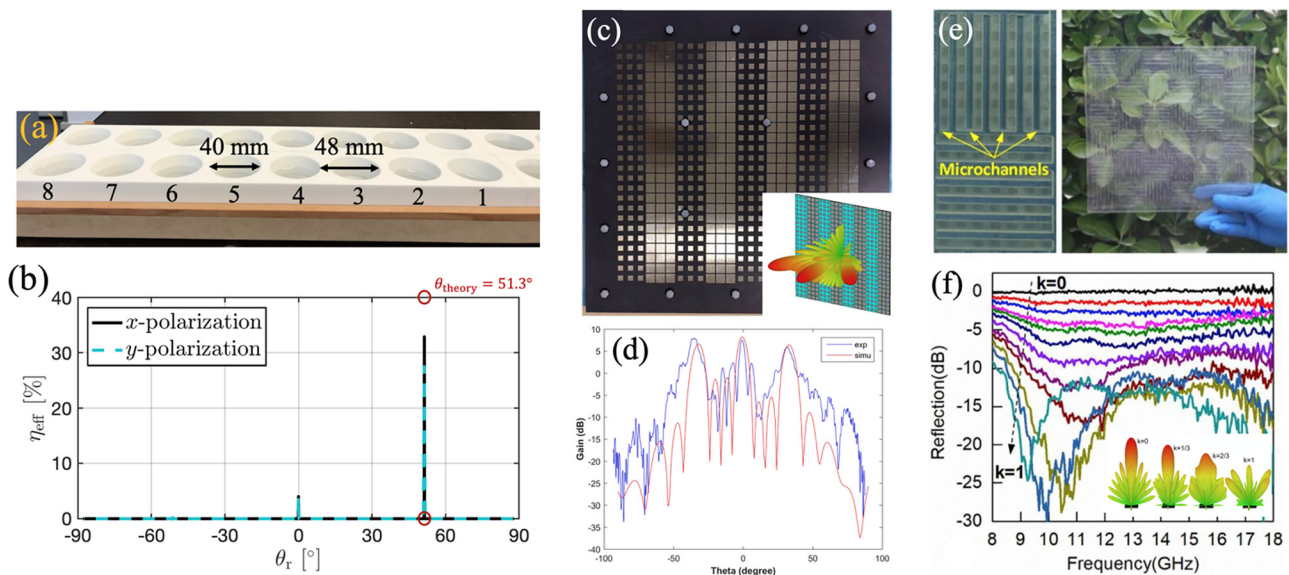
FIG. 5. Reflection control with WB MS reflectarrays. (a) and (b) MS reflectarray in the form of cylindrical water inclusions in a Rohacell 51 HF host backed with ground conducting plane. (a) Photograph of the fabricated MS. (b) The reflection efficiency as a function of the reflection angle for x- and y-polarized plane waves at normal incidence. Reprinted with permission from Jacobsen et al., J. Phys. D: Appl. Phys. **53**, 505104 (2020). Copyright 2020 IOP Publishing.[36] (c) and (d) MS with tunable reflection properties through different water-filling coding sequences. Both distilled water and NaCl solutions are used for the filling. (c) Photograph of the fabricated MS with the coding sequence "01010101" and (d) the measured and simulated radiation pattern (gain in dB). The inset in (c) shows a sketch of the MS and the radiation pattern. Adapted with permission from Chen et al., Sci. Rep. **8**, 2070 (2018). Copyright 2018 Authors, licensed under a Creative Commons Attribution 34 license.[34] (e) and (f) Reflection tuning of transparent MS with microfluidic channels. (e) Photograph of the fabricated MS and (f) measured reflection spectra for different water-fillings. The inset in (f) shows the simulated far-field scattering. Adapted with permission from Pang et al., Smart Mater. Struct. **29**, 115018 (2020). Copyright 2020 The IOP Publishing.[37]

substrate and a metallic ground conducting plane. Reflection was controlled by varying the water salinity. Furthermore, the radiation pattern could be tailored by reconfiguration of the metal coding pattern. In Ref. 35, diodes were incorporated into the MS to introduce another means for tuning. The radiation pattern was altered by switching the bias voltage of the diodes between on and off.

A similar MS design was reported in Ref. 37, Figs. 5(e) and 5(f). The MS consisted of a periodic element with films of indium tin oxide (ITO) spaced with a PMMA substrate. Water inclusions were embedded into the substrate and were connected with microfluidic channels. Through rotation of the element, a checkered subarray pattern was constructed. The water inclusion volumes were varied illustrating dynamic tuning of the reflection, see Fig. 5(f). Interestingly, the MS is very transparent at visible frequencies making it possible to employ it in situations, where visual transparency is desired, while impeding microwaves.

WB MS reflectarrays show promising tunability and/or reconfigurability. However, many of them are slow, and the water losses cause modest efficiencies. Still, the purpose of using water is to make simple, cheap, and green alternatives to conventional devices.

E. Metamaterials

The high permittivity of water enables realization of MMs with very low filling ratios.[20,23] A WB MM consisting of water-filled cylindrical containers with tunable properties was proposed in Ref. 23, see Figs. 6(a) and 6(b). By changing the permittivity of water and/or filling

of the cylindrical containers, the effective material parameters can be tuned. Refractive indices between 1 and 2 over a broad frequency band and with filling ratios less than 0.07 were achieved. The MM is simple and cheap and can be applied for transformation optics, lenses, or demonstration of wave physics.

A simple MM composed of metallic frames and water cylinders exhibits effective properties of a negative refractive index material.[33] Such materials, not naturally existing in nature, have attracted much attention in recent years with the potential of realizing devices such as lenses and waveguides that can go beyond the diffraction limit.[144] A magnetic dipole is excited in the water cylinders, which provides the negative magnetic response. The metallic frame brings the equivalent negative permittivity, and the effective refractive index is calculated to be -1.0 at 3.4 GHz. The experimental setup as shown in Fig. 6(d) is composed of a TEM rectangular waveguide with the MM placed in between the transmitter and the receiver of the waveguide. The MM has a flat surface toward the transmitter, whereas the surface toward the receiver is inclined by 11°. The simulated and measured normalized electric field along a line parallel to the MM is shown in Fig. 6(e). The incidence wave is mostly refracted in the opposite direction than normally happens with natural materials. This is the consequence of the negative effective refractive index.

WB MMs have been few in numbers thus far, which is not surprising due to the losses in water. To minimize the losses, non-resonant inclusions were applied in Ref. 23 whereas in Ref. 33 the MM are not a full 3-D periodic material. A WB MM capable of topological transitions was proposed in Ref. 22 and consists of water-coated
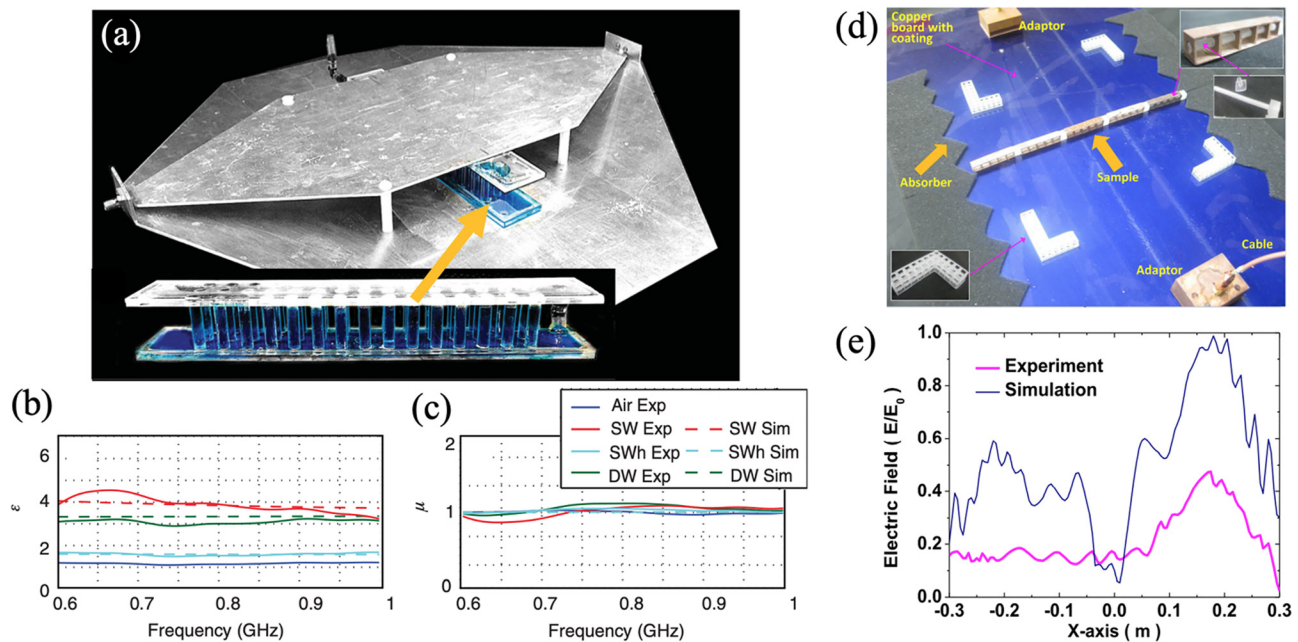
FIG. 6. (a)–(c) Demonstration of WB MM consisting of non-resonant water-filled cylindrical containers. Tuning of the MM is demonstrated by changing of water content as well the salinity level of water. (a) shows photographs of the MM and the experimental setup consisting of an open TEM waveguide. (b) and (c) show the effective permittivity and permeability spectra, respectively, for air and different fillings of saltwater (SW) and distilled water (DW). Adapted with permission from Liu *et al.*, Phys. Rev. B **89**, 245132 (2014). Copyright 2014 AIP Publishing.[23] (d) and (e) Metamaterial structure with an equivalent negative refractive index. (d) Photograph of the experiment composed of the metamaterial placed in a TEM waveguide. (e) Simulated and measured normalized electric field as along the axis parallel to the metamaterial. Reprinted with permission from Cai *et al.*, J. Appl. Phys. **122**, 184101 (2017). Copyright 2017 AIP Publishing.[33]

copper wires embedded in a ceramic host medium. By exploiting water permittivity's temperature dependence, potential of tuning the dispersion of the MM from being elliptic to flat and further to hyperbolic was demonstrated. However, we must emphasize that the water losses were neglected in the study, and thus the real response of the MM remains missing.

IV. ANTENNAS

The first WB antenna was proposed and demonstrated by Kingsley and O'Keefe in 1999.[80] It is a dielectric resonator antenna (DRA) composed of a water-filled (distilled) cylindrical polyvinyl chloride (PVC) container with an aluminum plate on the outer side. The container was placed on a conducting ground plane with five switchable coaxial monopole antenna feeds enabling beam-steering capabilities. Afterward, several WB antenna designs have been proposed, see Table I. Some exploit the high permittivity of distilled water,[80,85–91,93–96,98,102,105–107,110–113,116,118,119] while other utilize the conductivity of saltwater.[81,83,84,92,97,99,100,104,108,109,117,121,123–126] An example of the latter is shown in Figs. 7(a) and 7(b).[103,114] It is a monopole antenna composed of a continuous stream of seawater pumped out via a nozzle. In transmission state, an electric current is induced in the seawater stream with a magnetic feed consisting of circular ferrite magnets. Through control of the height of the seawater stream, the operational frequency is tuned between 2 and 400 MHz.

Another type of a WB antenna is shown in Figs. 7(c) and 7(d).[94] It is a water-loaded dipole antenna consisting of copper strips embedded into a water-filled box. The water allows for shrinking of the dipole antenna, which normal size is half of the free-space wavelength (λ_0), however, on the cost of reduced total efficiency. The prototype shown in Fig. 7(c) is approximately $\lambda_0/4$ in dimension and operates at around 0.2 GHz. By changing the temperature of the water, the antenna can be frequency-tuned as shown by the reflection coefficient

spectrum in Fig. 7(d). As the temperature increases, the total efficiency increases slightly stemming from the lower water absorption losses. The efficiency reduction due to the increased water volume was also investigated showing significant reduction for box thicknesses greater than $0.04\lambda_0$. For higher frequencies, this bound is even lower. A transparent WB antenna is shown in Figs. 7(e) and 7(f). It consists of a small metallic feed surrounded by circular patches of water, see the image in Fig. 7(e).[105] The antenna operates around 2.4 GHz with excellent matching (reflection coefficient below −20 dB) and modest realized gain (above –5 dB), see Fig. 7(f).

Many WB antennas are designed with a large metallic ground conducting plane, which limits their applications, see, e.g., Figs. 8(a)–8(c). Instead, a patch of water can be employed as demonstrated with the WB patch antenna in Fig. 7(e).

In many antenna applications, a signal is desired to be transmitted/received in/from a specific direction. Therefore, antennas with more directive radiation, and thus higher gain, must be used. Such Yagi-Uda WB antennas[118,121] and array WB antennas[117,122] have been reported. A microstrip patch antenna loaded with a MS embedded with fluidic channels and operating at 2.62 GHz is shown in Figs. 8(a)–8(c). The beam of the antenna can be steered through reconfiguration of the water-fillings in the fluidic channels, see Fig. 8(c). Not surprisingly, the gain is the highest, when the channels are without water (mode II). Adding water to the fluidic channels allows for steering of the beam, albeit halving the maximum gain. Nonetheless, the antenna constitutes a simple and compact alternative for beam-steering without the need for active electronic components.

A different approach toward increased gain can be achieved in compact DRAs with simultaneous excitation of multiple modes.[141] A subwavelength WB Huygens DRA was demonstrated in Ref. 93 where balanced magnetic and electric modes were excited in the DRA at 350 MHz. As a result, Kerker's condition is satisfied, see
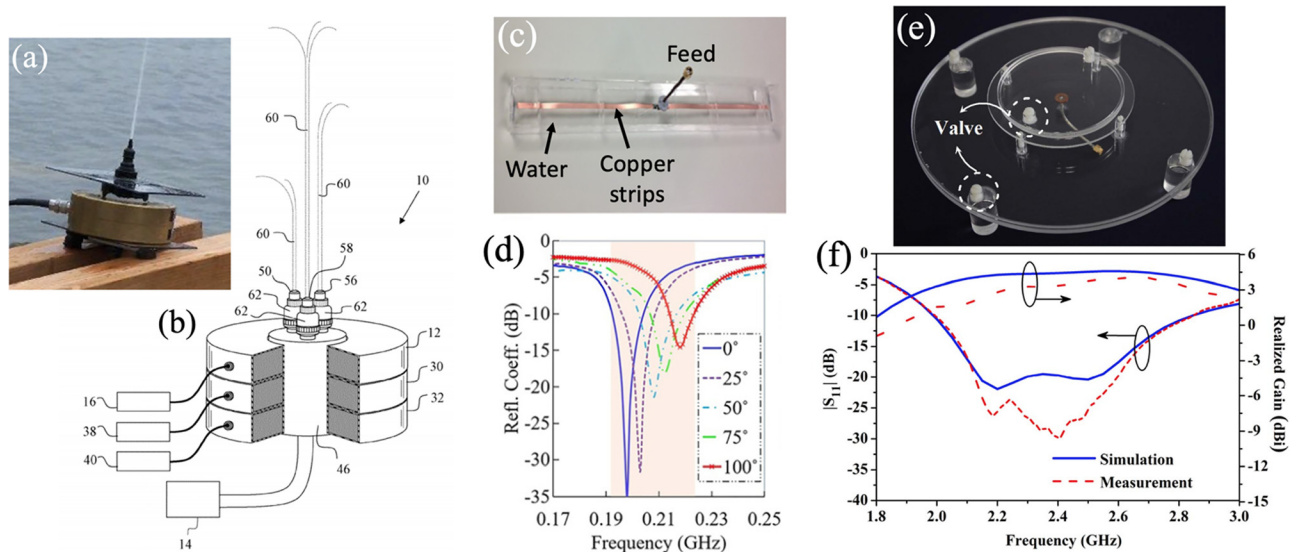
FIG. 7. WB microwave antennas. (a) Photograph and (b) schematic of a seawater antenna. Figures (a) and (b) are taken from Refs. 103 and 114, respectively. (c) Photograph of a water-loaded dipole antenna with the temperature-tuning capabilities shown in (d). Reprinted with permission from Mobashsher *et al.*, Appl. Phys. Lett. **110**, 253503 (2017). Copyright 2017 AIP Publishing.[94] (e) Photograph of a transparent WB patch antenna with (f) the measured and simulated reflection coefficient and realized gain spectra. Reprinted with permission from Sun *et al.*, IEEE Trans. Antennas Propag. **65**, 4478 (2017). Copyright 2017 IEEE.[105]
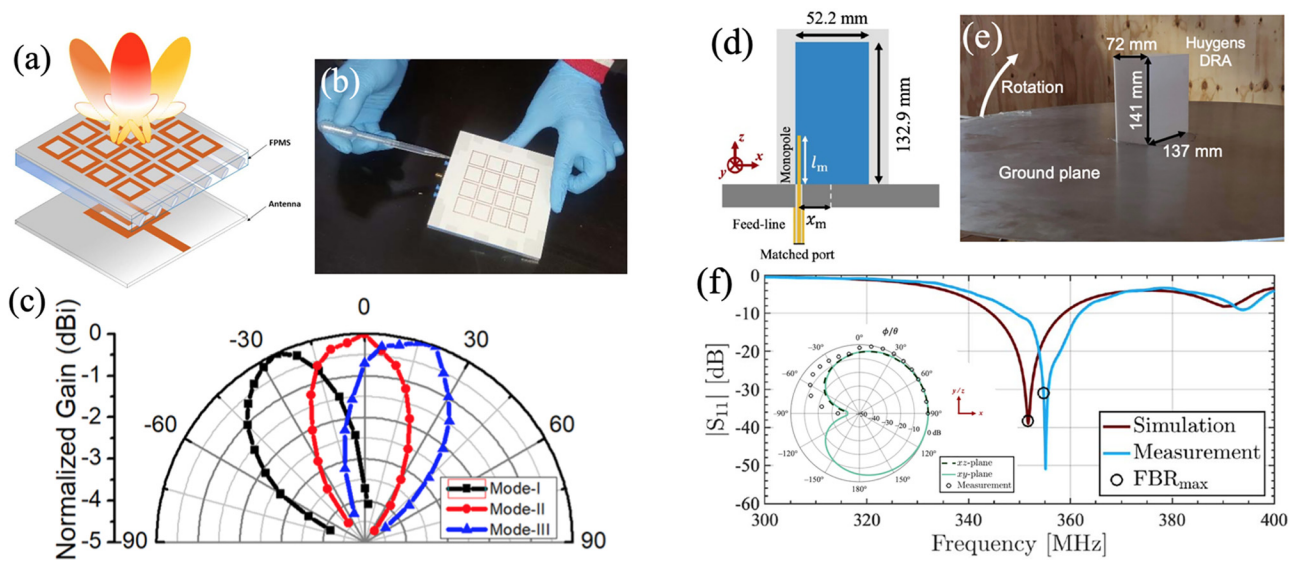
FIG. 8. Directive WB microwave antennas. (a) Sketch and (b) photograph of a beam-steering antenna with a WB MS. (c) Measured radiation pattern (normalized gain) for different water-fillings of the fluidic channels in the MS. Reprinted with permission from Naqvi *et al.*, IEEE Trans. Antennas Propag. **67**, 3704 (2019). Copyright 2019 IEEE.[117] (d) Sketch and (e) photograph of a WB Huygens DRA. (f) The simulated and measured reflection coefficient spectra with the inset showing the simulated and measured radiation pattern. Adapted with permission from Jacobsen *et al.*, IEEE Open J. Antennas Propag. **1**, 493 (2020). Copyright 2020 Authors, licensed under a Creative Commons Attribution (CC BY) license.[93]

Figs. 8(d)–8(f). The DRA comprises a short monopole antenna fed against a large ground conducting plane and encapsulated by a rectangular cuboid-shaped distilled water volume. The two excited dipole modes provided the DRA with twice the directivity as compared to a single dipole mode. The radiated power is diverted in one direction, providing an excellent front-to-back radiation ratio of around 40 dB. Furthermore, the DRA was self-matched to a 50 Ohm load with a very low reflection coefficient of approximately –40 dB.

The general issue with WB antennas is their reduced efficiencies due to the absorption losses in water. As the absorbed power is proportional to the square of the electric field magnitude, cf. Eq. (2), the small DRAs with high intensity fields suffer most from these losses. This was investigated for an electrically small WB hemispherical DRA in Ref. 90 with a size 18 times smaller than the free-space wavelength. Designed for 300 MHz operation, the effeciency was only 30%, whereas, when designed for 1 GHz operation, the efficiency is reduced threefold due to the increased water losses at higher frequencies.

V. RF COMPONENTS AND WAVEGUIDES

Fluidic microwave components display a way toward tunable passive microwave components. Mostly liquid-metal has been employed in a wide variety of component types, see review.[145] A few WB components have been demonstrated, and some of them are shown in Fig. 9.[128,129,146] A coplanar waveguide (CPW) with a water drop placed on top was examined in Ref. 128, see Figs. 9(a) and 9(b). By moving the drop, the wave response could be switched between the transmission and reflection states. Instead of a drop atop of the CPW, the CPW line can be suspended in water for absorption of waves.

A WB RF tuner was demonstrated in Ref. 129. Through different fillings of the small cavities in a CPW, the impedance of the line was tuned, see Fig. 9(c). As a proof of concept, the RF tuner was connected to an RF amplifier, which could be frequency-tuned with different cavity filling combinations, Fig. 9(d).

Additionally, we want to mention a field-effect transformer (FET) with a water drop atop presented in Ref. 146. The electrostatic characteristics of the FET were investigated. With the water drop, the FET could support rapid bias changes, high on/off current ratios, near-ideal sub-threshold swing, and enhanced short-channel behavior. Such a FET would be interesting to characterize on microwave frequencies.

VI. STRUCTURES WITH INTRIGUING MODES

Dynamic toroidal moments with a high Q-factor attracted a great deal of attention since their first demonstration.[147] For efficient excitation, such resonant modes require complex structures. A MS composed of clusters of four cylindrical water inclusions was demonstrated to exhibit a toroidal dipole around 1 and 2.5 GHz,[32,76] see Figs. 10(a)–10(d). At first, enhancement in the transmission was used to point on the excitation of the toroidal moment, Fig. 10(d). Later, the final proof of the existence of the toroidal dipole was done by the near field characterization.[76] Toroidal dipoles are dark modes (i.e., non-radiating), and thus their applications are limited, for example to absorbers and sensing.

In recent years, BICs have become a very hot topic within photonics and acoustics,[148,149] whereas only a few have been realized at microwave frequencies.[150–152] A BIC is a perfectly confined resonant mode of a system open for radiation. Theoretically, it possesses an infinite Q-factor, and is, therefore, of great interest for many applications including sensing, energy harvesting, lasing, etc. BICs can be classified according to the number of eigenmodes involved in the scattering process (single or multiple) as well as to the nature of their underlying interference mechanisms (symmetry-enabled or accidental BICs).
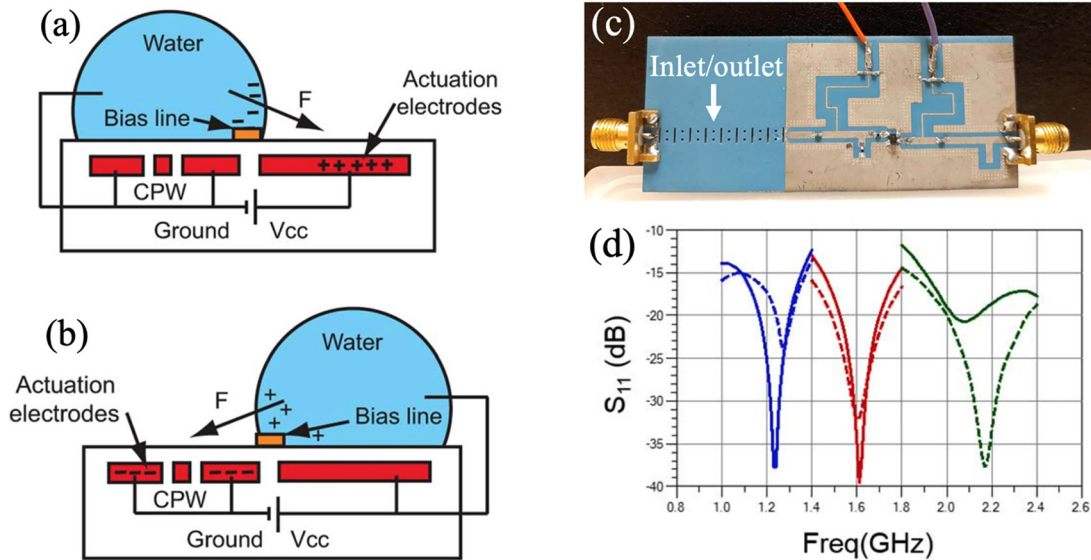
FIG. 9. RF components utilizing water. (a) and (b) Sketches of a water drop placed on a coplanar waveguide with different biases for on/off switching of guided waves. Reprinted with permission from Chen et al., IEEE Trans. Microwave Theory Tech. **55**, 2919 (2007). Copyright 2007 IEEE.[128] (c) Photograph of a RF tuner integrated with a RF amplifier and (d) reflection coefficient spectra.[129] The solid (dashed) lines show the simulation (measurement) results for different fillings of the cavities. Adapted with permission from Bahloul et al., IEEE Trans. Microwave Theory Tech. **68**, 3308 (2020). Copyright 2020 IEEE.[129]

When losses are present and/or symmetry is broken,[153] the BIC is turned into a quasi-BIC, resulting in a sharp Fano line shape in the radiation spectrum. A general problem of BIC structures is that all of their experimental realizations to date have inherently relied on very large arrays requiring large footprints. Thus, it certainly limits their applications when enhanced local density of states is on demand, for example in sensing. If only a few elements are included in a BIC array, the Q-factor is limited to a few dozens, which can be easily achieved with several more conventional modes.

Very recently, a novel symmetry-protected BIC structure has been demonstrated.[130] It is composed of a single metallic resonator placed in a rectangular waveguide, see Figs. 10(e)–10(g). Due to the symmetry of the resonator, the natural modes of the waveguide could not couple to a mode existing in the configuration, and thus a BIC emerged. To break the symmetry, a water drop was added asymmetrically atop of the resonator. Thus, the BIC was turned into a quasi-BIC, revealed by the measured reflection coefficient in a simple tabletop experiment, Figs. 10(f) and 10(g). The response depends on the shape, volume, position, temperature, and salinity of the water drop. These dependencies were utilized to make highly advanced sensing analyses including the dissolution of salt crystals in water and the evaporation of tiny water volumes from the drop. Such simple, well-controlled, and cost-effective approach being quite universal can be transferred to the lower (RF) and higher (photonics) frequency ranges with a row of promising applications.

VII. APPLICATIONS AND OUTLOOK

WB devices have the potential to be simple, cheap, bio-friendly, and tunable alternatives for many microwave applications. They find relevance in today's increasing focus on recyclability and low environmental footprint of products. So far, numerous WB devices of different

functionalities have been demonstrated showcasing advanced and diverse electromagnetic wave control with simple materials. Some WB devices contain rare and/or expensive materials. In these cases, the benefits of using water vanish, and thus, it can be exchanged with low-loss dielectrics instead.

The advantages of using water include a broad potential of dynamical reconfigurability of devices based on shape flexibility, provided by water's liquid state, easiness of volume tuning, temperature-dependent complex permittivity and strongly nonlinear interplay of self-heating of water volumes due to absorption, and changes in permittivity caused by this. Water's high permittivity allows the realization of highly compact water resonators with several tuning possibilities. The losses in water reduce the total scattering of these water resonators, as well as WB devices, however, concurrently the frequency bandwidth is increased. The progresses within 3D-printing technology enable easy and efficient fabrication of advanced host containers for water of peculiar shapes on demand. In particular, WB MSs that are configured with arrays of water inclusions are well suited for 3D-printing, see, e.g., Fig. 4(f).

Thus far, the most elaborated application of WB MS has been microwave absorbers. The area of WB MS absorbers has already matured offering various thin and flat alternatives to conventional absorbers. Therefore, as the forthcoming natural step we anticipate their implementations in real systems, such as in the case of rasorbers,[64,65] combination of radomes with absorbers. Besides, flexible and highly absorptive surfaces of anechoic chambers, camouflaging of big reflecting surfaces and transparent windows terminating all microwave radiation are likely to be the first among potential applications. Typically, the absorbers in anechoic chambers are pyramidal polyurethane foam blocks loaded with carbon particles, which pose a potential health risk to direct contact personnel. Furthermore, such foam blocks
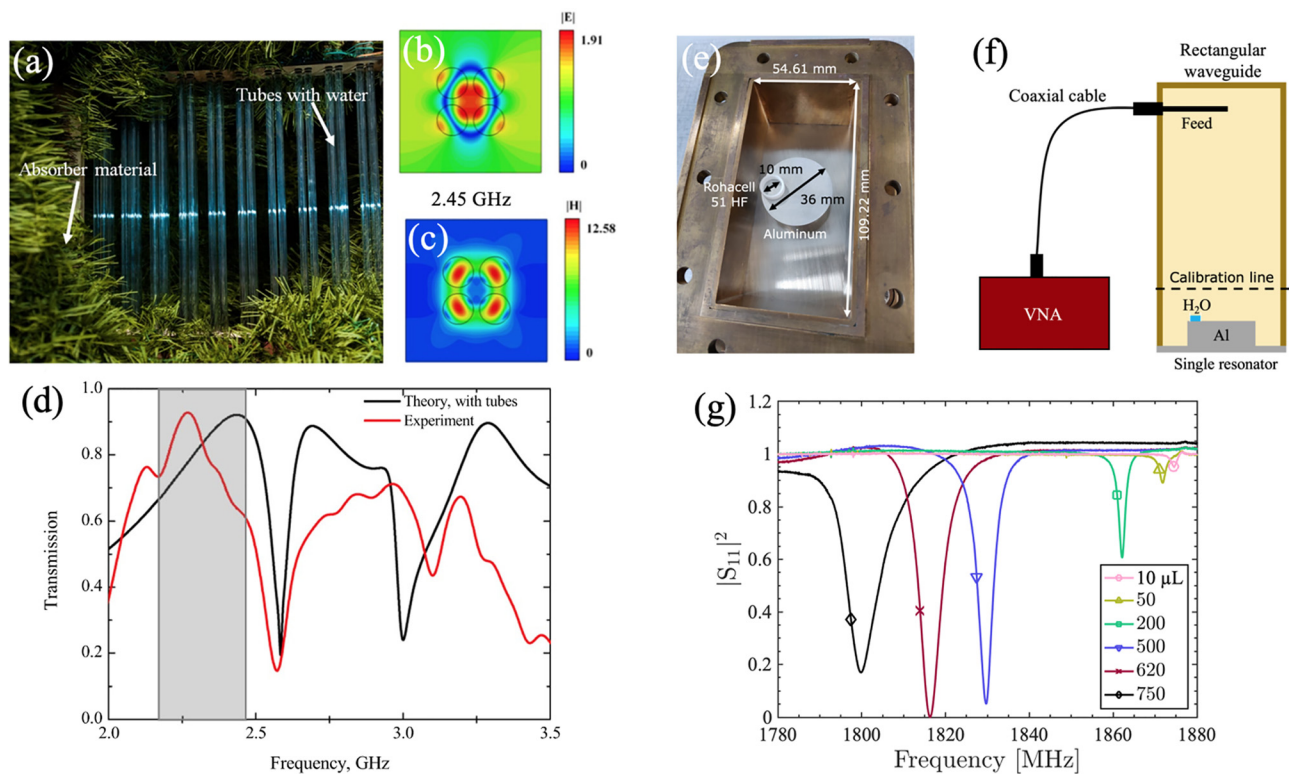
FIG. 10. (a)–(d) Demonstration of toroidal modes in an array composed of clusters of four cylindrical containers filled with water. (a) shows a photograph of the fabricated array with absorbing materials around it. (b) and (c) show the electric (top) and magnetic (bottom) field magnitudes in one cluster of cylinders. (d) shows the transmission spectra with the gray area indicating the frequency band of the toroidal mode. Reprinted with permission from Stenishchev *et al.*, Sci. Rep. **7**, 9468 (2017). Copyright 2017 Authors, licensed under a Creative Commons Attribution (CC BY) license.[32] (e)–(g) A boundary-induced BIC for advanced sensing. (e) Photograph of the fabricated resonator placed in a rectangular waveguide section. (f) Sketch of the experimental setup and (g) normalized measured reflection coefficient for different water volume insertions. Reproduced with permission from Jacobsen *et al.*, *Conference Lasers Electro-Optics*. Copyright 2021 Authors.[130]

are very expensive and bulky. Here, WB MS absorbers can serve as bio-friendly, recyclable and flexible alternatives. As for the other types of WB MSs, the low efficiency and weather-instability constitute major challenges, which must be resolved before they can compete with existing technology.

WB antennas are still viewed as impracticable in real-life implementations by microwave engineers due to their low stability and/or reduced efficiency. Several ways to overcome these limitations have been presented, and hopefully Challenges of WB antennas applications will be lifted off in the nearest years. Other liquids, including salty water, both with dielectric and conducting properties are becoming the point of attention.[127] As a matter of fact, a sea antenna has already been piloted for military usage.[103]

Recent research efforts have demonstrated new possibilities of water as a new element in conventional systems.[129,130] In particular, the single resonator structure with a localized BIC, in which water was used to break the symmetry of the system, enables the possibility of practical microwave BICs. Besides the obvious advantages of simple and low-cost microwave setups, such localized BICs can overcome many intrinsic limitations of the more traditional microwave modes. They may thus open the possibility of truly novel and highly tunable microwave devices including MSs for advanced microwave control

and sensing. We believe that the WB circuitry and just single water elements adding functionalities to the systems are in the beginning of the research boom, which will be driven in a long term by the UN proclaimed goals on global sustainability and human-friendly environment.

DATA AVAILABILITY

Data sharing is not applicable to this article as no new data were created or analyzed in this study.

REFERENCES

[1]H. A. Swenson and H. L. Baldwin, *A primer on water quality, 1990 reprint* (United States Geological Survey, U.S. GPO, 1965).
[2]NASA, *Ocean Worlds*, https://www.nasa.gov/specials/ocean-worlds/ (Accessed 24 September 2021).
[3]P. Ball, *Life's Matrix: A Biography of Water*, 1st ed. (Farrar, Straus & Giroux, New York, 1999).
[4]J. D. Smith, C. D. Cappa, K. R. Wilson, B. M. Messer, R. C. Cohen, and R. J. Saykally, Science **306**, 851 (2004).
[5]F. Franks, *Water: A Comprehensive Treatise*, 1st ed. (Plenum Press, New York, 1975), Vol. 1–5.
[6]I. Popov, P. Ben Ishai, A. Khamzin, and Y. Feldman, Phys. Chem. Chem. Phys. **18**, 13941 (2016).

7 D. Laage and J. T. Hynes, Science **311**, 832 (2006).

8 M. Sharma, R. Resta, and R. Car, Phys. Rev. Lett. **98**, 247401 (2007).

9 W. J. Ellison, J. Phys. Chem. Ref. Data **36**, 1–18 (2007).

10 R. L. Fulton, J. Chem. Phys. **130**, 204503 (2009).

11 H. J. Bakker and J. L. Skinner, Chem. Rev. **110**, 1498 (2010).

12 N. C. Burtch, H. Jasuja, and K. S. Walton, Chem. Rev. **114**, 10575 (2014).

13 J. O. Richardson, C. Pérez, S. Lobsiger, A. A. Reid, B. Temelso, G. C. Shields, Z. Kisiel, D. J. Wales, B. H. Pate, and S. C. Althorpe, Science **351**, 1310 (2016).

14 D. C. Elton and M. Fernandez-Serra, Nat. Commun. **7**, 10193 (2016).

15 D. C. Elton, Phys. Chem. Chem. Phys. **19**, 18739 (2017).

16 P. Ball, Nat. **452**, 291 (2008).

17 M. V. Rybin, D. S. Filonov, P. A. Belov, Y. S. Kivshar, and M. F. Limonov, Sci. Rep. **5**, 8774 (2015).

18 B. I. Popa and S. A. Cummer, Nat. Mater. **14**, 363 (2015).

19 A. Andryieuski, S. M. Kuznetsova, S. V. Zhukovsky, Y. S. Kivshar, and A. V. Lavrinenko, Sci. Rep. **5**, 13535 (2015).

20 M. V. Rybin, D. S. Filonov, K. B. Samusev, P. A. Belov, Y. S. Kivshar, and M. F. Limonov, Nat. Commun. **6**, 10102 (2015).

21 Z. Shen, H. Yang, X. Huang, and Z. Yu, J. Opt. **19**, 115101 (2017).

22 M. A. Gorlach, M. Song, A. P. Slobozhanyuk, A. A. Bogdanov, and P. A. Belov, Phys. Status Solidi RRL **10**, 900 (2016).

23 L. Liu, A. R. Katko, D. Li, and S. A. Cummer, Phys. Rev. B **89**, 245132 (2014).

24 M. Odit, P. Kapitanova, A. Andryieuski, P. Belov, and A. V. Lavrinenko, Appl. Phys. Lett. **109**, 11901 (2016).

25 X. Yang, D. Zhang, S. Wu, Y. Yin, L. Li, K. Cao, and K. Huang, Sci. Rep. **7**, 3190 (2017).

26 A. V. Lavrinenko, R. E. Jacobsen, S. Arslanagic, S. Kuznetsova, A. Andryieuski, M. Odit, and P. Kapitanova, in *Proceedings of the 47th European Microwave Conference* (IEEE, 2017), pp. 492–495.

27 A. V. Lavrinenko, R. E. Jacobsen, and S. Arslanagic, in *Proceedings of the 48th European Microwave Conference* (IEEE, 2018), pp. 819–822.

28 R. E. Jacobsen, A. V. Lavrinenko, and S. Arslanagic, IEEE Antennas Wireless Propag. Lett. **17**, 571 (2018).

29 R. E. Jacobsen, S. Arslanagic, and A. V. Lavrinenko, in *Swedish Microwave Days* (Lund, 2018).

30 M. Odit, A. Saynskyi, I. Munina, and P. Belov, J. Phys.: Conf. Ser. **1092**, 012103 (2018).

31 P. Kapitanova, A. Sayanskiy, M. Odit, A. Miroshnichenko, A. Lavrinenko, and P. Belov, in *20th Anniversary International Conference on Transparent Optical Networks* (IEEE, 2018).

32 I. V. Stenishchev and A. A. Basharin, Sci. Rep. **7**, 9468 (2017).

33 X. Cai, S. Zhao, M. Hu, J. Xiao, N. Zhang, and J. Yang, J. Appl. Phys. **122**, 184101 (2017).

34 L. Chen, H. L. Ma, X. J. Song, Y. Ruan, and H. Y. Cui, Sci. Rep. **8**, 2070 (2018).

35 L. Chen, H. L. Ma, Y. Ruan, and H. Y. Cui, J. Appl. Phys. **125**, 23107 (2019).

36 R. E. Jacobsen, J. Ø. Nielsen, A. V. Lavrinenko, and S. Arslanagic, J. Phys. D: Appl. Phys. **53**, 505104 (2020).

37 Y. Pang, M. Mo, Y. Li, B. Qu, S. Xia, S. Qu, and Z. Xu, Smart Mater. Struct. **29**, 115018 (2020).

38 M. Odit, A. Sayanskiy, V. Asadchy, and P. Belov, in *IEEE International Symposium on Antennas Propagation Society and USNC National Radio Science Meeting (APSURSI 2018)—Proceedings* (IEEE, 2018), pp. 773–774.

39 Y. J. Yoo, S. Ju, S. Y. Park, Y. Ju Kim, J. Bong, T. Lim, K. W. Kim, J. Y. Rhee, and Y. Lee, Sci. Rep. **5**, 14018 (2015).

40 Q. Song, W. Zhang, P. C. Wu, W. Zhu, Z. X. Shen, P. H. J. Chong, Q. X. Liang, Z. C. Yang, Y. L. Hao, H. Cai, H. F. Zhou, Y. Gu, G. Q. Lo, D. P. Tsai, T. Bourouina, Y. Leprince-Wang, and A. Q. Liu, Adv. Opt. Mater. **5**, 1601103 (2017).

41 J. Zhao, S. Wei, C. Wang, K. Chen, B. Zhu, T. Jiang, and Y. Feng, Opt. Express **26**, 8522 (2018).

42 J. Xie, W. Zhu, I. D. Rukhlenko, F. Xiao, C. He, J. Geng, X. Liang, R. Jin, and M. Premaratne, Opt. Express **26**, 5052 (2018).

43 Y. Shen, J. Zhang, Y. Pang, J. Wang, H. Ma, and S. Qu, Opt. Express **26**, 15665 (2018).

44 Y. Pang, Y. Shen, Y. Li, J. Wang, Z. Xu, and S. Qu, J. Appl. Phys. **123**, 155106 (2018).

45 Z. Shen, X. Huang, H. Yang, T. Xiang, C. Wang, Z. Yu, and J. Wu, J. Appl. Phys. **123**, 225106 (2018).

46 D. J. Gogoi and N. S. Bhattacharyya, J. Appl. Phys. **124**, 75106 (2018).

47 P. J. Bradley, M. O. M. Torrico, C. Brennan, and Y. Hao, Sci. Rep. **8**, 14490 (2018).

48 D. J. Gogoi and N. S. Bhattacharyya, J. Appl. Phys. **125**, 125107 (2019).

49 H. F. Zhang, X. L. Tian, G. B. Liu, and X. R. Kong, IEEE Access **7**, 25827 (2019).

50 E. Yang, F. Yang, J. Pei, X. Zhang, S. Liu, and Y. Deng, J. Phys. D: Appl. Phys. **52**, 395501 (2019).

51 Y. Pang, J. Wang, Q. Cheng, S. Xia, X. Y. Zhou, Z. Xu, T. J. Cui, and S. Qu, Appl. Phys. Lett. **110**, 104103 (2017).

52 Z. Wu, X. Chen, Z. Zhang, L. Heng, S. Wang, and Y. Zou, Appl. Phys. Express **12**, 57003 (2019).

53 F. Yang, J. Gong, E. Yang, Y. Guan, X. He, S. Liu, X. Zhang, and Y. Deng, Appl. Phys. A **125**, 149 (2019).

54 J. Xie, S. Quader, F. Xiao, C. He, X. Liang, J. Geng, R. Jin, W. Zhu, and I. D. Rukhlenko, IEEE Antennas Wireless Propag. Lett. **18**, 536 (2019).

55 H. Xiong and F. Yang, Opt. Express **28**, 5306 (2020).

56 Q. Liang, Z. Yang, J. Guo, Z. Li, T. Chen, and D. Li, J. Mater. Sci. Mater. Electron. **31**, 19242–19247 (2020).

57 X. Zhang, F. Yan, X. Du, W. Wang, and M. Zhang, AIP Adv. **10**, 55211 (2020).

58 B. X. Khuyen, V. T. H. Hanh, B. S. Tung, V. D. Lam, Y. J. Kim, Y. Lee, H. T. Tu, and L. Y. Chen, Crystals **10**, 415 (2020).

59 X. Zhang, D. Zhang, Y. Fu, S. Li, Y. Wei, K. Chen, X. Wang, and S. Zhuang, IEEE Antennas Wireless Propag. Lett. **19**, 821 (2020).

60 Q. Wang, K. Bi, and S. Lim, IEEE Access **8**, 175998 (2020).

61 H. Zhang, F. Ling, H. Wang, Y. Zhang, and B. Zhang, Opt. Commun. **463**, 125394 (2020).

62 W. Zhu, I. D. Rukhlenko, F. Xiao, C. He, J. Geng, X. Liang, M. Premaratne, and R. Jin, Opt. Express **25**, 15737 (2017).

63 K.-L. Zhang, X.-D. Cheng, Y.-J. Zhang, M. Chen, H. Chen, Y. Yang, W.-L. Song, and D. Fang, ACS Appl. Mater. Interfaces **10**, 40815 (2018).

64 S. K. Patel, K. H. Shah, and J. S. Sonagara, Waves Random Complex Media **30**, 328 (2018).

65 X. Yan, X. Kong, Q. Wang, L. Xing, F. Xue, Y. Xu, S. Jiang, and X. Liu, IEEE Trans. Antennas Propag. **68**, 6162 (2020).

66 D. J. Gogoi and N. S. Bhattacharyya, J. Appl. Phys. **122**, 175106 (2017).

67 H. Huang, H. Yang, Z. Shen, J. Chen, H. Lin, and Z. Yu, J. Phys. D: Appl. Phys. **50**, 385304 (2017).

68 Z. Han, J. Zhao, and Y. Feng, in *IEEE 6th Asia-Pacific Conference on Antennas and Propagation (APCAP 2017)—Proceeding* (IEEE, 2017), p. 8420663.

69 Y. Shen, J. Zhang, Y. Pang, L. Zheng, J. Wang, H. Ma, and S. Qu, Sci. Rep. **8**, 4423 (2018).

70 Y. Shen, J. Zhang, S. Sui, Y. Jia, Y. Pang, J. Wang, H. Ma, and S. Qu, J. Phys. D: Appl. Phys. **51**, 485301 (2018).

71 J. Ren and J. Y. Yin, Opt. Mater. Express **8**, 2060 (2018).

72 R. E. Jacobsen, S. Arslanagic, and A. V. Lavrinenko, in *Proceedings of the International Symposium on Electromagnetics Theory* (IEEE, 2019), p. 8931459.

73 R. E. Jacobsen, S. Arslanagic, and A. V. Lavrinenko, in *URSI International Symposium on Electromagnetic Theory* (IEEE, 2019), pp. 1–4.

74 R. E. Jacobsen, S. Arslanagic, and A. V. Lavrinenko, URSI Radio Sci. Lett. **1**, 1–4 (2019).

75 P. Kapitanova, V. Ternovski, A. Miroshnichenko, N. Pavlov, P. Belov, Y. Kivshar, and M. Tribelsky, Sci. Rep. **7**, 731 (2017).

76 N. Pavlov, I. Stenishchev, A. Ospanova, P. Belov, P. Kapitanova, and A. Basharin, Phys. Status Solidi B **257**, 1900406 (2020).

77 E. Motovilova, S. Sandeep, M. Hashimoto, and S. Y. Huang, IEEE Access **7**, 90304 (2019).

78 H. K. Khattak, P. Bianucci, and A. D. Slepkov, Proc. Natl. Acad. Sci. U. S. A. **116**, 4000 (2019).

79 H. W. Wu, H. J. Chen, H. F. Xu, R. H. Fan, and Y. Li, Sci. Rep. **8**, 8817 (2018).

[80]S. P. Kingsley and S. G. O'Keefe, IEE Proc. Radar, Sonar Navig. **146**, 121 (1999).

[81]M. Wang and Q. X. Chu, IEEE Antennas Wireless Propag. Lett. **17**, 799 (2018).

[82]L. Xing, X. Meng, L. Yang, B. Xu, and Y. Pan, in *IEEE International Workshop on Antenna Technology (IWAT2018)* (IEEE, 2018), pp. 1–3.

[83]Y.-H. Qian and Q.-X. Chu, IEEE Antennas Wireless Propag. Lett. **16**, 1360 (2017).

[84]L. Xing, J. Zhu, Q. Xu, D. Yan, and Y. Zhao, IEEE Antennas Wireless Propag. Lett. **18**, 2140 (2019).

[85]A. Singh, I. Goode, and C. E. Saavedra, IEEE Antennas Wireless Propag. Lett. **18**, 856 (2019).

[86]J. J. Liang, G. L. Huang, K. W. Qian, S. L. Zhang, and T. Yuan, IEEE Access **6**, 34804 (2018).

[87]M. Wang and Q. X. Chu, IEEE Antennas Wireless Propag. Lett. **18**, 402 (2019).

[88]L. Xing, Q. Xu, J. Zhu, Y. Zhao, S. Aljaafreh, C. Song, and Y. Huang, IEEE Antennas Propag. Mag. **63**, 61 (2021).

[89]Y. Chen and C. F. Wang, in *IEEE International Symposium on Antennas and Propagation Society (AP-S)* (Institute of Electrical and Electronics Engineers Inc., 2014), pp. 848–849.

[90]R. E. Jacobsen, A. V. Lavrinenko, and S. Arslanagic, Appl. Sci. **9**, 4848 (2019).

[91]S. G. O'Keefe and S. P. Kingsley, IEEE Antennas Wireless Propag. Lett. **6**, 533 (2007).

[92]H. Fayad and P. Record, Electron. Lett. **42**, 133 (2006).

[93]R. E. Jacobsen, A. V. Lavrinenko, and S. Arslanagic, IEEE Open J. Antennas Propag. **1**, 493 (2020).

[94]A. T. Mobashsher and A. Abbosh, Appl. Phys. Lett. **110**, 253503 (2017).

[95]M. Lapierre, Y. M. M. Antar, A. Ittipiboon, and A. Petosa, IEEE Microwave Wireless Compon. Lett. **15**, 7 (2005).

[96]M. Zou, Z. Shen, and J. Pan, Appl. Phys. Lett. **108**, 14102 (2016).

[97]G. H. Huff, D. L. Rolando, P. Walters, and J. McDonald, IEEE Antennas Wireless Propag. Lett. **9**, 288 (2010).

[98]Z. Gong, C. Bartone, F. Yang, and J. Yao, Appl. Phys. Lett. **112**, 113501 (2018).

[99]Z. Chen and H. Wong, IEEE Trans. Antennas Propag. **66**, 444 (2018).

[100]L. Xing, Y. Huang, Q. Xu, and S. Alja'Afreh, Microwave Opt. Technol. Lett. **57**, 2160 (2015).

[101]R. E. Jacobsen, M. H. Vandborg, A. V. Lavrinenko, and S. Arslanagic, in 14th European Conference on Antennas and Propagation, Copenhagen, Denmark (2020).

[102]Z. Ren, S. S. Qi, Z. Hu, Z. Shen, and W. Wu, IEEE Trans. Antennas Propag. **67**, 6770 (2019).

[103]J. Pavlus, see https://www.technologyreview.com/2010/11/18/198879/navy-antenna-using-seawater-instead-of-metal/ for "Navy Antenna Using Seawater Instead of Metal."

[104]G. Li, Y. Huang, G. Gao, C. Yang, Z. Lu, and W. Liu, Int. J. Electron. **105**, 645 (2018).

[105]J. Sun and K. M. Luk, IEEE Trans. Antennas Propag. **65**, 4478 (2017).

[106]J. Sun and K. M. Luk, IEEE Access **7**, 122964 (2019).

[107]Y. Li and K. M. Luk, IEEE Access **3**, 274 (2015).

[108]Z. Chen and H. Wong, IEEE Trans. Antennas Propag. **65**, 2157 (2017).

[109]M. Konca and P. A. Warr, IEEE Trans. Antennas Propag. **63**, 5280 (2015).

[110]J. D. Barrera and G. H. Huff, IEEE Trans. Antennas Propag. **62**, 4008 (2014).

[111]C. Murray and R. R. Franklin, IEEE Antennas Wireless Propag. Lett. **13**, 1449 (2014).

[112]Y. H. Qian and Q. X. Chu, IEEE Antennas Wireless Propag. Lett. **16**, 2179 (2017).

[113]H. Tang and J. X. Chen, IEEE Access **5**, 20470 (2017).

[114]D. W. S. Tam, US8368605 (2013), https://patents.google.com/patent/US8368605B1/en.

[115]S. K. Patel and Y. Kosta, Microwave Opt. Technol. Lett. **60**, 318 (2018).

[116]L. Xing, Y. Huang, Q. Xu, S. Alja'Afreh, and T. Liu, IEEE Antennas Wireless Propag. Lett. **15**, 174 (2016).

[117]A. H. Naqvi and S. Lim, IEEE Trans. Antennas Propag. **67**, 3704 (2019).

[118]Y.-H. Qian and Q.-X. Chu, Microwave Opt. Technol. Lett. **59**, 1608 (2017).

[119]R. Zhou, H. Zhang, and H. Xin, IET Microwave, Antennas Propag. **8**, 255 (2014).

[120]C. Song, E. L. Bennett, J. Xiao, A. Alieldin, K. M. Luk, and Y. Huang, IEEE Trans. Antennas Propag. **67**, 4907 (2019).

[121]S. Wang, Z. Hu, W. Wang, S. Qi, and W. Wu, Int. J. RF Microwave Comput. Eng. **28**, e21399 (2018).

[122]R.-G. Fan, Y.-H. Qian, and Q.-X. Chu, Microwave Opt. Technol. Lett. **59**, 2284 (2017).

[123]C. Borda-Fortuny, L. Cai, K. F. Tong, and K. K. Wong, IEEE Access **7**, 95058 (2019).

[124]C. Hua, Z. Shen, and J. Lu, IEEE Trans. Antennas Propag. **62**, 5968 (2014).

[125]C. Hua and Z. Shen, IEEE Trans. Antennas Propag. **63**, 5185 (2015).

[126]L. Xing, Y. Huang, Y. Shen, S. Al Ja'afreh, Q. Xu, and R. Alrawashdeh, IET Microwave, Antennas Propag. **9**, 735 (2015).

[127]E. Motovilova and S. Y. Huang, Materials **13**, 1863 (2020).

[128]C. H. Chen and D. Peroulis, IEEE Trans. Microwave Theory Tech. **55**, 2919 (2007).

[129]D. Bahloul and A. B. Kouki, IEEE Trans. Microwave Theory Tech. **68**, 3308 (2020).

[130]R. E. Jacobsen, A. Krasnok, S. Arslanagic, A. V. Lavrinenko, and A. Alú, in *Conference Lasers Electro-Optics* (Optical Society of America, San Jose, California, 2021), pp. 1–2.

[131]C. F. Bohren and D. R. Huffman, *Absorption and Scattering of Light by Small Particles*, 1st ed. (John Wiley & Sons, Hoboken, New York, 1983).

[132]D. Tzarouchis and A. Sihvola, Appl. Sci. **8**, 184 (2018).

[133]A. Petosa and A. Ittipiboon, IEEE Antennas Propag. Mag. **52**, 91 (2010).

[134]S. Jahani and Z. Jacob, Nat. Nanotechnol. **11**, 23 (2016).

[135]A. G. Webb, J. Magn. Reson. **216**, 107 (2012).

[136]A. Keshavarz and Z. Vafapour, IEEE Sens. J. **19**, 1519 (2019).

[137]A. Strogryn, IEEE Trans. Microwave Theory Technol. **19**, 733 (1971).

[138]J. D. Jackson, *Classical Electrodynamics*, 3rd ed. (John Wiley & Sons, New York, 1999).

[139]ROHACELL, see https://www.rohacell.com for "ROHACELL HF—High-Performance Structural Foam Cores."

[140]R. Alaee, R. Filter, D. Lehr, F. Lederer, and C. Rockstuhl, Opt. Lett. **40**, 2645 (2015).

[141]R. W. Ziolkowski, Phys. Rev. X **7**, 031017 (2017).

[142]N. Yu, P. Genevet, M. A. Kats, F. Aieta, J.-P. Tetienne, F. Capasso, and Z. Gaburro, Science **334**, 333 (2011).

[143]S. B. Glybovski, S. A. Tretyakov, P. A. Belov, Y. S. Kivshar, and C. R. Simovski, Phys. Rep. **634**, 1–72 (2016).

[144]M. Kadic, G. W. Milton, M. van Hecke, and M. Wegener, Nat. Rev. Phys. **1**, 198 (2019).

[145]K. Entesari and A. P. Saghati, IEEE Microwave Mag. **17**, 50 (2016).

[146]Y. Huang, E. Sutter, L. M. Wu, H. Xu, L. Bao, H. J. Gao, X. J. Zhou, and P. Sutter, ACS Appl. Mater. Interfaces **10**, 23198 (2018).

[147]T. Kaelberer, V. A. Fedotov, N. Papasimakis, D. P. Tsai, and N. I. Zheludev, Science **330**, 1510 (2010).

[148]C. W. Hsu, B. Zhen, A. D. Stone, J. D. Joannopoulos, and M. Soljacic, Nat. Rev. Mater. **1**, 16048 (2016).

[149]A. Krasnok, D. Baranov, H. Li, M.-A. Miri, F. Monticone, and A. Alú, Adv. Opt. Photonics **11**, 892 (2019).

[150]T. Lepetit, E. Akmansoy, J. P. Ganne, and J. M. Lourtioz, Phys. Rev. B **82**, 195307 (2010).

[151]T. Lepetit and B. Kanté, Phys. Rev. B **90**, 241103 (2014).

[152]Z. F. Sadrieva, M. A. Belyakov, M. A. Balezin, P. V. Kapitanova, E. A. Nenasheva, A. F. Sadreev, and A. A. Bogdanov, Phys. Rev. A **99**, 053804 (2019).

[153]K. Koshelev, S. Lepeshov, M. Liu, A. Bogdanov, and Y. Kivshar, Phys. Rev. Lett. **121**, 193903 (2018).